https://doi.org/10.5194/essd-2023-446
Preprint. Discussion started: 20 December 2023

Open Access Earth System Science Data Discussions

A Global Forest Burn Severity Dataset from Landsat Imagery (2003–2016)

Kang He[1,2], Xinyi Shen[3], and Emmanouil N. Anagnostou[1,2]

[1]Department of Civil and Environmental Engineering, University of Connecticut, Storrs, CT 06269, USA
[2]Eversource Energy Center, University of Connecticut, Storrs, CT 06269, USA
[3]School of Freshwater Sciences, University of Wisconsin, Milwaukee, Milwaukee, WI 53204, USA

Correspondence to: Emmanouil N. Anagnostou (emmanouil.anagnostou@uconn.edu)

Abstract: Forest fires, while destructive and dangerous, are important to the functioning and renewal of ecosystems. Over the past two decades, large-scale, severe forest fires have become more frequent globally, and the risk is expected to increase as fire weather and drought conditions intensify. To improve quantification of the intensity and extent of forest fire damage, we have developed a Global Forest Burn Severity (GFBS) database of information on the amounts of biomass that were consumed by fire between 2003 and 2016. To build it, we used the Fire Atlas product to determine when and where forest fires occurred during that period and then overlaid the available Landsat surface reflectance products to obtain pre-fire and post-fire normalized burn ratios (NBRs) for each burned pixel, designating the difference between them as dNBR and the relative difference as RdNBR. Using the CONUS-wide Composite Burn Index (CBI) as a ground truth, we evaluated the performance of GFBS relative to the performance of the existing MODIS-based global burn severity dataset (MOSEV). The results showed that dNBR of GFBS was more strongly correlated with CBI ($R^2 = 0.4$) than dNBR of MOSEV ($R^2 = 0.08$). RdNBR of GFBS also exhibited better agreement with CBI ($R^2 = 0.31$) than RdNBR of MOSEV ($R^2 = 0.04$). At global scale, while the dNBR and RdNBR spatial patterns extracted by GFBS were similar to those of MOSEV, MOSEV tended to provide higher burn severity levels than GFBS. We attribute this difference to variations in reflectance values and the different spatial resolutions of the two satellites.

1. Introduction

In recent years, many regions around the world have experienced an increase in the frequency, intensity, and extent of wildfires (Doerr and Santín, 2016; Shukla et al., 2019; Dupuy et al., 2020). Wildfires are now among the most popular research topics as a result of this rising global concern, which is further heightened by changes expected in fire regimes as a consequence of changes in climate and land use (Moreira et al., 2020). While most wildfires occur in grasslands and savannas (Scholes and Archer, 1997; Abreu et al., 2017), forest fires are more dangerous and destructive and perhaps of greater interest because of their importance to the functioning and renewal of ecosystems (Flannigan et al., 2000; Nasi et al., 2002; Flannigan et al., 2006). Changes brought by the warming climate, which has

https://doi.org/10.5194/essd-2023-446
Preprint. Discussion started: 20 December 2023

dried fuels and lengthened fire seasons across the globe (Jolly et al., 2015), are also particularly significant to forested ecosystems with abundant fuels (Kasischke and Turetsky, 2006; Aragão et al., 2018).

With the rapid development of remote sensing techniques, more frequent observations from satellites facilitate the monitoring of global fire activities. The valuable information they provide at fine spatial and temporal resolutions can be used to study the number and size distributions of individual fires (Archibald and Roy, 2009; Hantson et al., 2015; Oom et al., 2016), fire shapes (Nogueira et al., 2016; Laurent et al., 2018), and locations of ignition points (Benali et al., 2016; Fusco et al., 2016). Among the most widely accepted techniques are those based on the Moderate Resolution Imaging Spectrometer (MODIS) (Chuvieco et al., 2016), which retrieves information on the entire Earth in 36 spectral bands every one to two days. The MODIS-derived burn area (BA) products are essential for ascertaining the patterns of fire occurrence, extent, propagation (Rodrigues and Febrer, 2018), and frequency (Andela et al., 2019). Based on these products, an essential indicator called "burn severity" has been derived for determining the degree of biomass consumption and the overall impact of fire on ecosystems (Keeley, 2009).

Traditionally, burn severity could be quantified from satellite sensors through spectrum information. The changes caused by fire to near-infrared (NIR) and shortwave infrared (SWIR) reflectance are highly sensitive to, respectively, canopy density and moisture content (Chuvieco, 2010). Several burn severity datasets based on this method have been generated and released. Regionally, the Monitoring Trends in Burn Severity (MTBS) dataset, which includes burn severity assessments for the contiguous United States (CONUS) and provides information on fire perimeters and severity classes, uses satellite data—specifically, Landsat imagery (Eidenshink et al., 2007). Similarly, the Canadian Landsat Burn Severity (CanLaBS) product uses Landsat imagery to assess, and map burn severity at a national scale (Guindon et al., 2021). Globally, MOdis burn SEVerity (MOSEV) has provided monthly burn severity data with global coverage at 500m spatial resolution, based on MODIS Terra and Aqua satellites (Alonso-González and Fernández-García, 2021). Despite the satellite those datasets used and the target those datasets for, products for assessing and mapping global forest burn severity based on Landsat (30m resolution) are not yet available. Such products would support advances in fire management strategies and ecosystem conservation efforts, leading to more resilient and sustainable landscapes.

In this paper we describe a new global dataset comprising information on burn severity derived at high spatial resolution from Landsat imagery from the period 2003–2016. This dataset represents a step forward in quantifying and analyzing wildfire impact on forest ecosystems worldwide. We begin with a section detailing the input data and the algorithm we used to process the dataset, as well as the analytical techniques employed. The next section presents the characteristics of the dataset and its performance in representing the distribution of forest fires. In the results section, we analyze the advantages and disadvantages of the dataset and set forth its main contributions to forest fire management strategies worldwide. The last section summarizes the primary findings and suggests possible implications of the dataset.

2. Data and Method

https://doi.org/10.5194/essd-2023-446
Preprint. Discussion started: 20 December 2023

Below we delineate the specifics of data input and pre-processing and the analytical techniques we employed to create the dataset. The Global Fire Atlas was the main source of global fire records, which we overlaid with annual land cover types from MCD12Q1 to determine when and where forest fires occurred. We then utilized the reflectance information from Landsat's satellite archives to calculate burn severity indices for the burned forest areas. Finally, we used the CONUS-wide Composite Burn Index (CBI) as a ground truth to evaluate the performance of GFBS relative to that of the existing MODIS-based global burn severity dataset (MOSEV).

2.1. Input data

The input data we used to build the GFBS dataset comprised the fire records available in the Global Fire Atlas for the years 2003–2016 and all Landsat images for the same period.

The Global Fire Atlas tracks the daily dynamics of individual fires globally to determine the time and location of ignition, area burned, and duration, as well as daily expansion, fireline length, velocity, and direction of spread. A detailed description of its underlying methodology is provided by Andela et al. (2019).

The Terra and Aqua combined Moderate Resolution Imaging Spectroradiometer (MODIS) Land Cover Type (MCD12Q1) Version 6.1 data product provides global land cover types at yearly intervals (**USGS, 2022**). With its global coverage and the insights, it offers into the planet's diversity of land cover types, the MCD12Q1 dataset is pivotal to various ecological and environmental studies.

Landsat 5,7,8 scene is a 16-day composite image with 7, 8, 11 surface reflectance bands. With its 30m resolution and global coverage, it provides a high-quality, atmospherically corrected snapshot of the Earth's surface. Use of the best available observations gathered over the 16-day period ensures the image is as clear and accurate as possible, minimizing issues, such as cloud cover, that can obscure the satellite's view. (https://developers.google.com/earth-engine/datasets/catalog/landsat).

2.2. Pre-processing

To pre-process the data, we first imported individual fire polygons from the Global Fire Atlas into the Google Earth Engine (GEE) and then collected the most recent Landsat images based on the tags demarcating the start and end times of each individual fire. We applied a cloud- and snow-masking algorithm to remove any snow, clouds, and their shadows from all imagery based on each sensor's pixel quality assessment band. By mosaicing the masked images, we created a composite with the smallest possible cloud and shadow extent (Google Earth Engine Developers, 2022). (https://developers.google.com/earth-engine/guides/landsat).

2.3. Algorithm overview

We estimated the burn severity indices in two steps, as shown in Figure 1: first, we calculated the normalized burn ratios (NBRs) from the mosaiced Landsat composites, and second, we selected the pre- and post-fire NBRs for each burned pixel to create burn severity indices—dNBR and RdNBR—based on the differences between the NBRs.

https://doi.org/10.5194/essd-2023-446
Preprint. Discussion started: 20 December 2023

In the first step, we determined the forest fire polygons using the Global Fire Atlas data associated with the MCD12Q1 land cover data and then utilized reflectance information from Landsat's satellite archives to obtain the forest fire NBRs from the Landsat composites.

In the second step, we used the pre- and post-fire dates by the Global Fire Atlas data to obtain the corresponding pre- and post-fire NBRs, which allowed us to create the burn severity indices—that is, dNBR and RdNBR—based on the respective differences between them.

We took additional steps to validate the performance of the dataset by comparing the CBIs over CONUS with those based on the MOSEV dataset. These steps are detailed in Sections 2.3.1, 2.3.2, and 2.3.3.

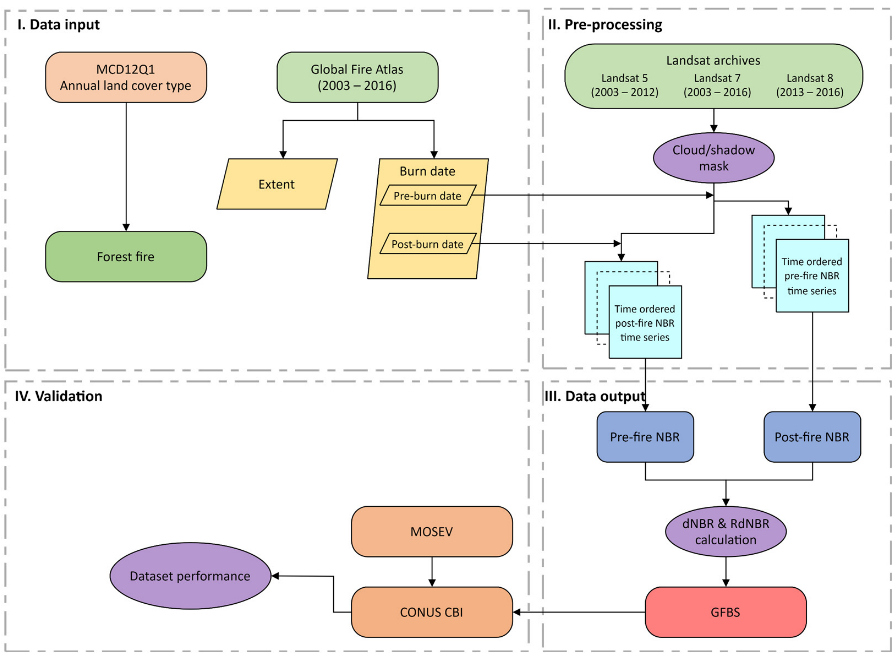

Figure 1. Methodology for building the GFBS database (2003–2016) and validation and comparison with the MOSEV benchmark.

2.3.1. Identification of global forest fires

To identify global forest fires, we first overlaid the fire polygons from the Global Fire Atlas with MCD12Q1 data from the corresponding year. Based on Annual International Geosphere-Biosphere Programme (IGBP) classifications of land cover, we identified a forest fire polygon within each area where we found forest to be the dominant land cover type within the fire extent—that is, wherever the proportion of burned pixels representing forest, including evergreen needleleaf forests, evergreen broadleaf forests, deciduous needleleaf forests, deciduous broadleaf forests, and mixed forests, was largest relative to the proportion of burned pixels for other land cover types, such as shrublands and grasslands.

https://doi.org/10.5194/essd-2023-446
Preprint. Discussion started: 20 December 2023

2.3.2. Estimation of the normalized burn ratio (NBR)

We calculated the normalized burn ratio (NBR) spectral index for each Landsat composite. according to the formula in Equation 1:

$$\text{NBR} = (\text{NIR} - \text{SWIR}) / (\text{NIR} + \text{SWIR}), \tag{1}$$

In Landsat series 4 through 7, we collected NIR information from Band 4 and SWIR information from Band 7. In Landsat 8, we collected NIR information from Band 5 and SWIR information from Band 7.

2.3.3. Estimation of dNBR and RdNBR

Having obtained burn area locations and burn dates from the Fire Atlas product, we selected from the Landsat 16-day time series valid pre-fire and post-fire NBR pixels that were, respectively, from the date most closely preceding the start date and the date most closely following the end date of each burned polygon within a three-month time window.

The dNBR index, calculated according to Key and Benson (2006) as shown in equation (2), is the reference burn severity spectral index used by the European Forest Fire Information System (https://effis.jrc.ec.europa.eu/about-effis) and by the United States' Monitoring Trends in Burn Severity program (https://www.mtbs.gov). Larger dNBR values indicate higher burn severity:

$$\text{dNBR} = \text{preNBR} - \text{postNBR} \tag{2}$$

RdNBR is another burn severity spectral index that is widely used, including by the United States' Monitoring Trends in Burn Severity program (https://www.mtbs.gov/, last access:1 May 2021). As formulated in equation (3) (Miller and Thode, 2007), higher RdNBR values indicate higher burn severity:

$$\text{RdNBR} = \text{dNBR}/\sqrt{|preNBR|} \tag{3}$$

2.4. Validation

To validate the GFBS database developed in this study, we used the ground-measured CONUS-wide Composite Burn Index from 2003 to 2016. CBI was developed by Key and Benson (2006) to assess the aboveground effects of fire on vegetation and soil land use types (i.e., burn severity). The index ranges continuously from 0.0 (unburned) to 3.0 (high severity). These values can be compared to satellite-derived burn severity data to develop regression equations (https://burnseverity.cr.usgs.gov/products/cbi). In this study, we used all available CBI values over CONUS to establish the regression relationship between CBI and the dNBR and RdNBR values of the GFBS database. We applied the coefficient of determination to evaluate the performance of GFBS relative to the corresponding performance of the MOSEV database, which is currently used to evaluate global burn severity.

https://doi.org/10.5194/essd-2023-446
Preprint. Discussion started: 20 December 2023

3. Results

3.1. Landsat mosaiced composites

Figure 2 (a) shows the number of forest fire polygons globally between 2003 and 2016, representing individual fire events, from the Global Fire Atlas dataset. Approximately 80,000 forest fire events occur in the world each year on average, with more than 90,000 happening in 2004 and more than 100,000 in 2003 and 2015, respectively. Figure 2 (a) also displays the availability of Landsat imagery covering the burn area where individual forest fires happened worldwide. From 2003 to 2012, Landsat 5 could provide images covering only 35% to 68% of the recorded forest fire events in the Global Fire Atlas, while Landsat 7 images could cover 83% to 93%. From 2013 to 2016, Landsat 7 images covered about 90% to 98% of the fire events, while Landsat 8 images covered more than 97%. The Landsat composites combining all available Landsat 5 and Landsat 7 images from 2003 to 2012 and Landsat 7 and Landsat 8 images from 2013 to 2016 significantly increased the number of forest fires shown by Landsat images, with coverage of the fire events ranging from 88% to 99%. Figure 2 (b) shows the distribution of the spatial coverage of cloud-free Landsat composites for individual fires from the Fire Atlas. We used a cloud and shadow removal algorithm to eliminate invalid poor-quality pixels from recorded forest fires, resulting in a line chart showing the distribution of the percentages of valid pixels to the total burn pixels in each year. Overall, the spatial coverage was above 72%, and the coverage has been above 85% since 2013, when Landsat 8 was launched.

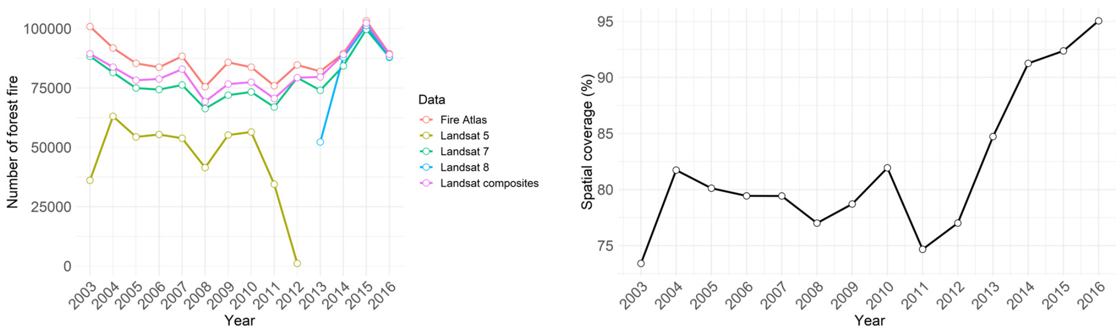

(a) (b)

Figure 2. (a) Numbers of individual fires from the Fire Atlas and available Landsat imagery; (b) Spatial coverage of cloud-free Landsat composites for individual fires from the Fire Atlas.

3.2. Validation against CBI

Figure 3 shows the spatial locations of available CBIs over CONUS from 2003 to 2016. Of the 1,315 ground-surveyed CBI reports for forest fires during that time, most came from western states, such as Arizona, Colorado, and Oregon, where forest fires are more frequent and severe. Fewer CBI records are available in eastern states, such as Florida and Georgia.

https://doi.org/10.5194/essd-2023-446
Preprint. Discussion started: 20 December 2023

Open Access Earth System Science Data Discussions

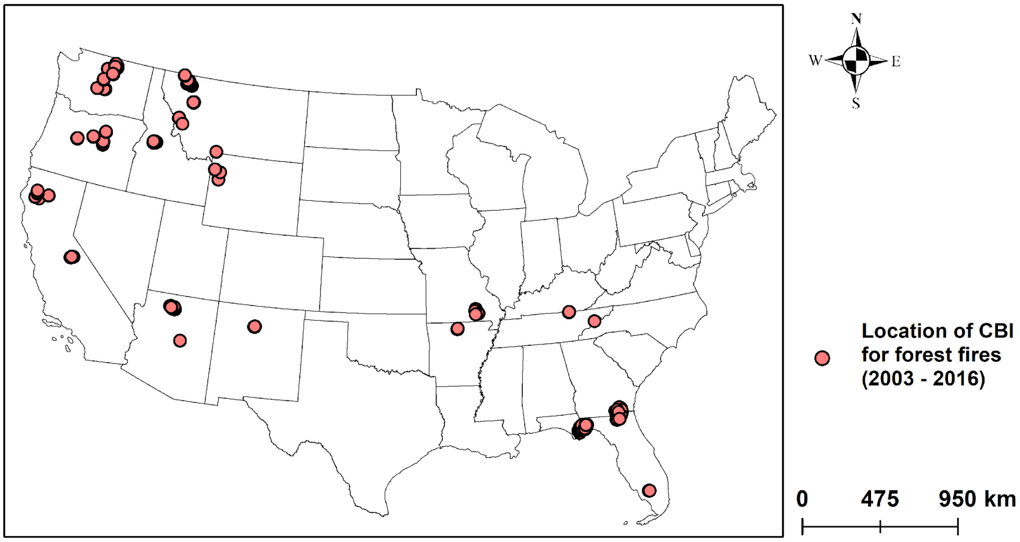

Figure 3. Spatial locations of forest fire CBIs over CONUS.

Figure 4 (a), (b), (c) and (d) shows the spatial patterns of dNBR over CONUS for the forest fires with the largest burn areas (referred to as annual maximum forest fire hereafter) in 2004, 2006, 2007, and 2013 respectively for which CBI records are available. The figures present the associated probability density functions (PDFs) of dNBR values from GFBS and MOSEV, along with spatial distribution maps of dNBR. The similarity in spatial patterns between GFBS burn severity and MOSEV burn severity is obvious. Significant differences occur, however, between GFBS dNBR and MOSEV dNBR. We found that, when we relied on MODIS products, MOSEV dNBR tended to underestimate the high severity and overestimate the low severity of the annual maximum forest fire in 2004, compared with GFBS dNBR. This could also be inferred from the PDFs, where MOSEV dNBR distributed more on the mean value of dNBR around 300, while GFBS dNBR distributed more on the extreme low and high values. For the annual maximum forest fire in 2007, especially, MOSEV dNBR greatly overestimated the severity levels compared to GFBS dNBR, a difference that was also reflected in the large deviation of mean dNBR values in the PDFs of dNBR for the GFBS and MOSEV datasets.

The density plot of dNBR in Figure 4 also clearly shows two peaks for GFBS dNBR, at around 100 (low severity) and 700 (high severity), for the annual maximum forest fire in 2006. MOSEV dNBR shows a single peak at around 500, indicating that MOSEV dNBR underestimated high severity while overestimating low severity, compared with GFBS dNBR. For the annual maximum forest fire in 2013, although the density plot presents two peaks for both GFBS and MOSEV dNBR, the corresponding dNBR values where the peaks are located differ. For GFBS dNBR, the two peaks are around 0 and 900, representing the low and high severity, respectively, while for MOSEV dNBR they are around 400 and 600.

https://doi.org/10.5194/essd-2023-446
Preprint. Discussion started: 20 December 2023

Open Access Earth System Science Data Discussions

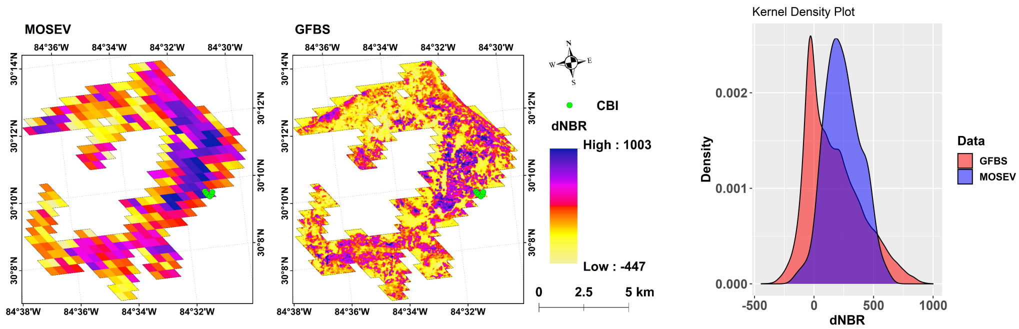

(a)

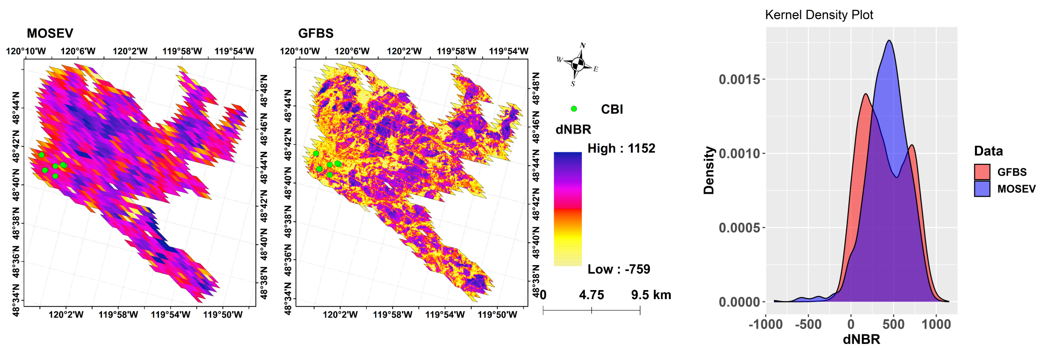

(b)

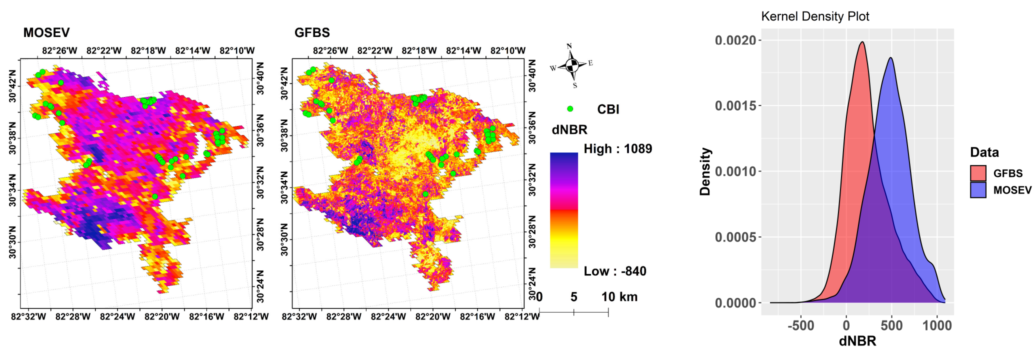

(c)

https://doi.org/10.5194/essd-2023-446
Preprint. Discussion started: 20 December 2023

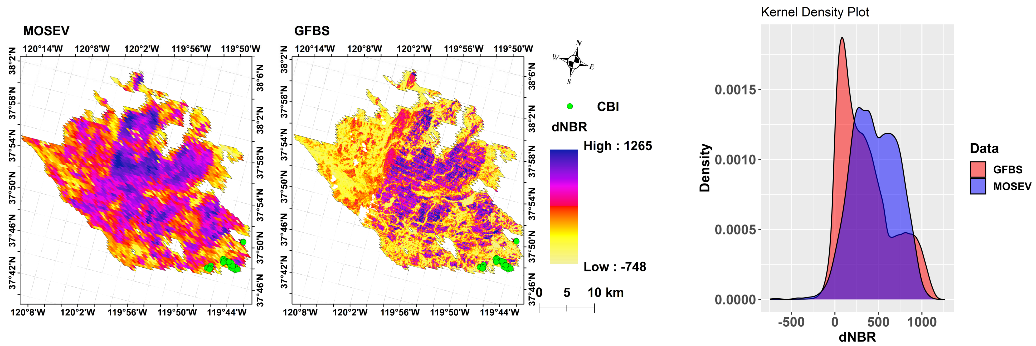

(d)

Figure 4. Spatial patterns of dNBRs for annual maximum fires over CONUS with distribution of probability density functions in (a) 2004, (b) 2006, (c) 2007, and (d) 2013, derived from the GFBS and MOSEV datasets.

Figure 5, panels (a), (b), (c), and (d), present the scatterplots of CBI against GFBS dNBR and MOSEV dNBR for the annual maximum forest fires in 2004, 2006, 2007, and 2013, respectively. For the annual maximum forest fire in 2004, the figure clearly shows a positive correlation with CBI ($R^2 = 0.21$) for GFBS dNBR, while we found no correlation for MOSEV dNBR. For the annual maximum forest fire in 2006, we found good agreement with the CBI for GFBS dNBR, with an R^2 value of 0.72, while the R^2 value was only 0.08 for MOSEV dNBR. Although correlation with CBI was poor for both GFBS and MOSEV dNBR for the annual maximum forest fire in 2007, the former still showed a positive trend to CBI, while the relationship for the latter was negative. For the annual maximum forest fire in 2013, GFBS dNBR ($R^2 = 0.52$) was more strongly correlated with CBI than MOSEV dNBR ($R^2 = 0.13$).

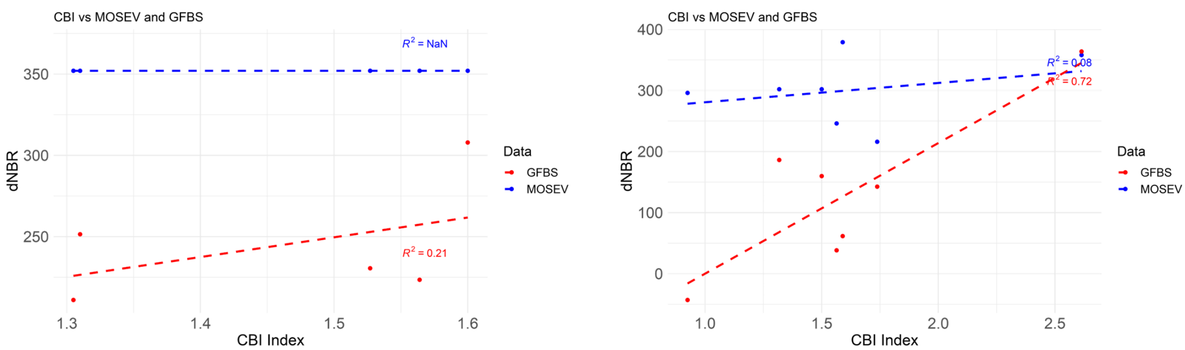

(a) (b)

https://doi.org/10.5194/essd-2023-446
Preprint. Discussion started: 20 December 2023

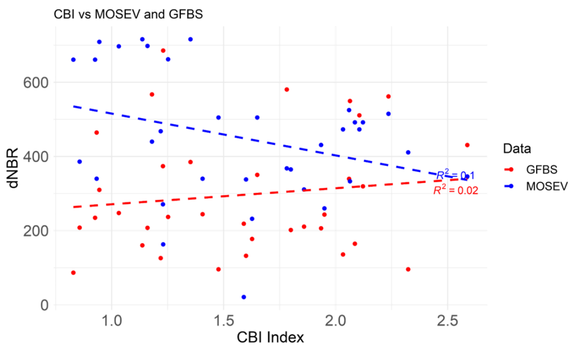

(c)

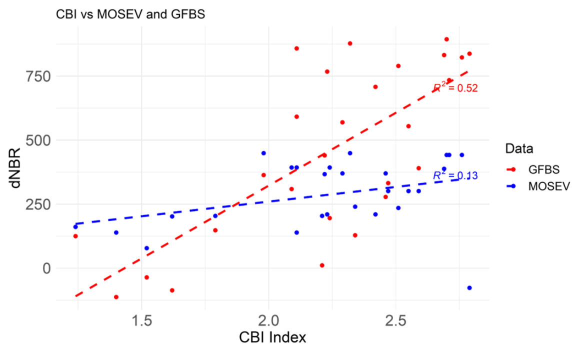

(d)

Figure 5. Scatterplots of CBI against dNBR of GFBS and MOSEV for annual maximum fires in (a) 2004, (b) 2006, (c) 2007, and (d) 2013.

Figure 6 (a), (b), (c) and (d) shows the spatial patterns of RdNBR for the forest fires over CONUS with the largest burn areas (referred to as annual maximum forest fire hereafter) in 2004, 2006, 2007, and 2013 respectively for which recorded CBIs are available. Like Figure 4, Figure 6 displays the spatial distribution maps of RdNBR from GFBS and MOSEV, along with the associated probability density functions (PDFs) of RdNBR values. The figure exhibits similar spatial patterns for GFBS and MOSEV dataset, but the burn severity level in terms of RdNBR differed. RdNBR for MOSEV data tended to be higher than for GFBS dNBR, which can be clearly seen in the density plots of GFBS and MOSEV RdNBRs that the mean RdNBR in the distribution of MOSEV is obviously larger than the mean RdNBR in the distribution of GFBS, for the annual maximum forest fires in 2003, 2006 and 2007. The density plots of GFBS and MOSEV RdNBR for the annual maximum forest fire in 2013 are largely overlapped, but MOSEV RdNBR distributes more on the mean values around 800 than GFBS RdNBR, while GFBS RdNBR distributes more on the extreme low and high values. These findings demonstrate that MOSEV RdNBR represents higher burn severity levels than GFBS RdNBR.

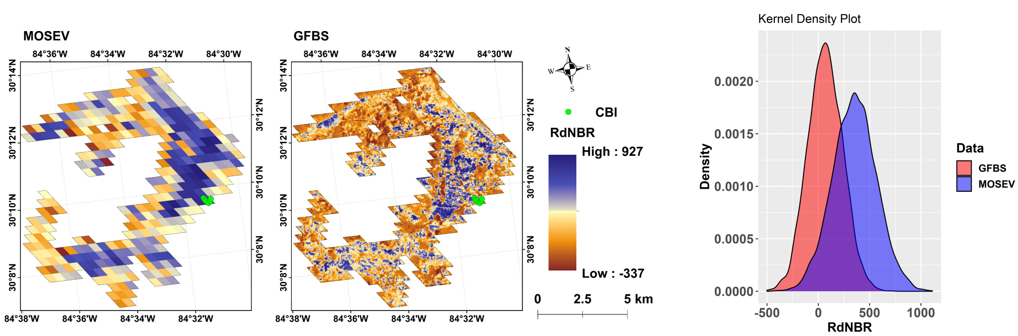

(a)

https://doi.org/10.5194/essd-2023-446
Preprint. Discussion started: 20 December 2023

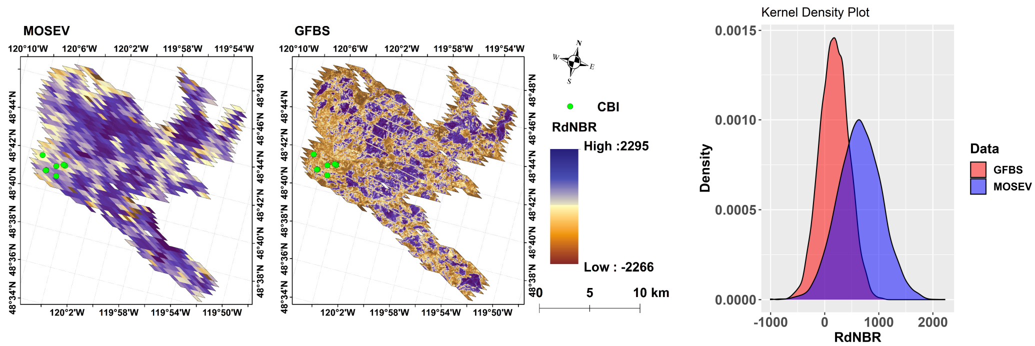

(b)

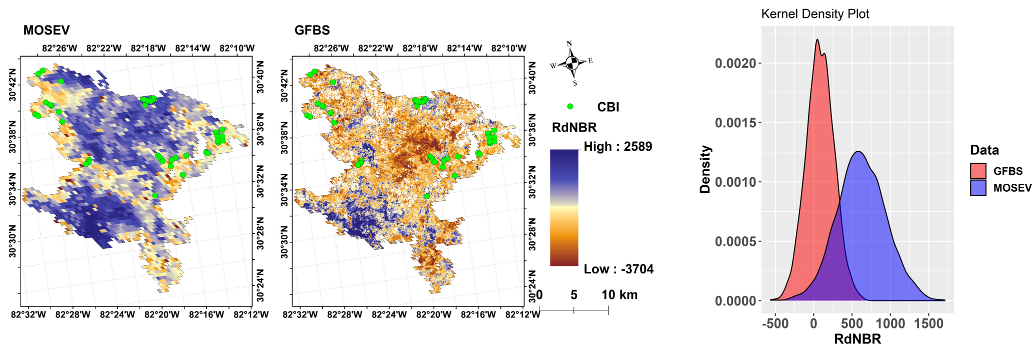

(c)

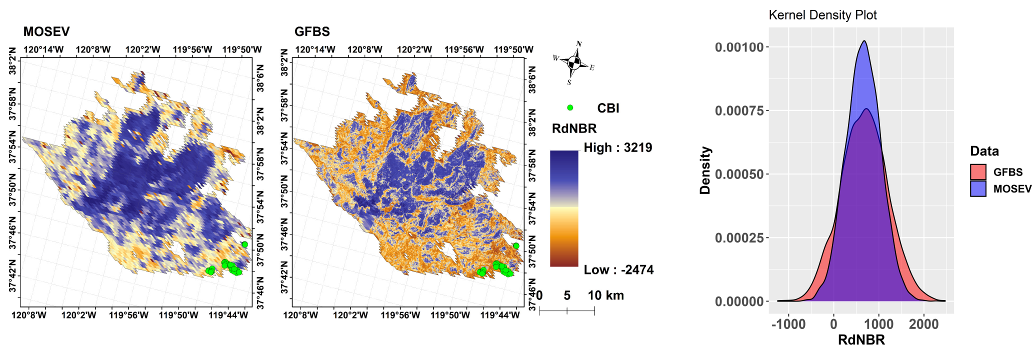

(d)

Figure 6. Spatial patterns of RdNBRs for annual maximum fires over CONUS with distribution of probability density functions in (a) 2004, (b) 2006, (c) 2007, and (d) 2013, derived from the GFBS and MOSEV datasets.

Figure 7, panels (a), (b), (c), and (d), present the scatterplots of CBI against GFBS RdNBR and MOSEV RdNBR for the annual maximum forest fires in 2004, 2006, 2007, and 2013, respectively. For the annual maximum

https://doi.org/10.5194/essd-2023-446
Preprint. Discussion started: 20 December 2023

forest fire in 2004, the figure shows a positive correlation with CBI (R^2 = 0.33) for GFBS dNBR, while we found no correlation for MOSEV dNBR. For the annual maximum forest fire in 2006, we found good agreement with the CBI for GFBS dNBR with an R^2 value of 0.72, while the R^2 value was only 0.03 for MOSEV dNBR. Although correlation with CBI was poor for both GFBS and MOSEV dNBR for the annual maximum forest fire in 2007, the former still showed a positive trend to CBI, while the relationship for the latter was negative. For the annual maximum forest fire in 2013, GFBS dNBR (R^2 = 0.55) was more strongly correlated with CBI than MOSEV dNBR (R^2 = 0.16).

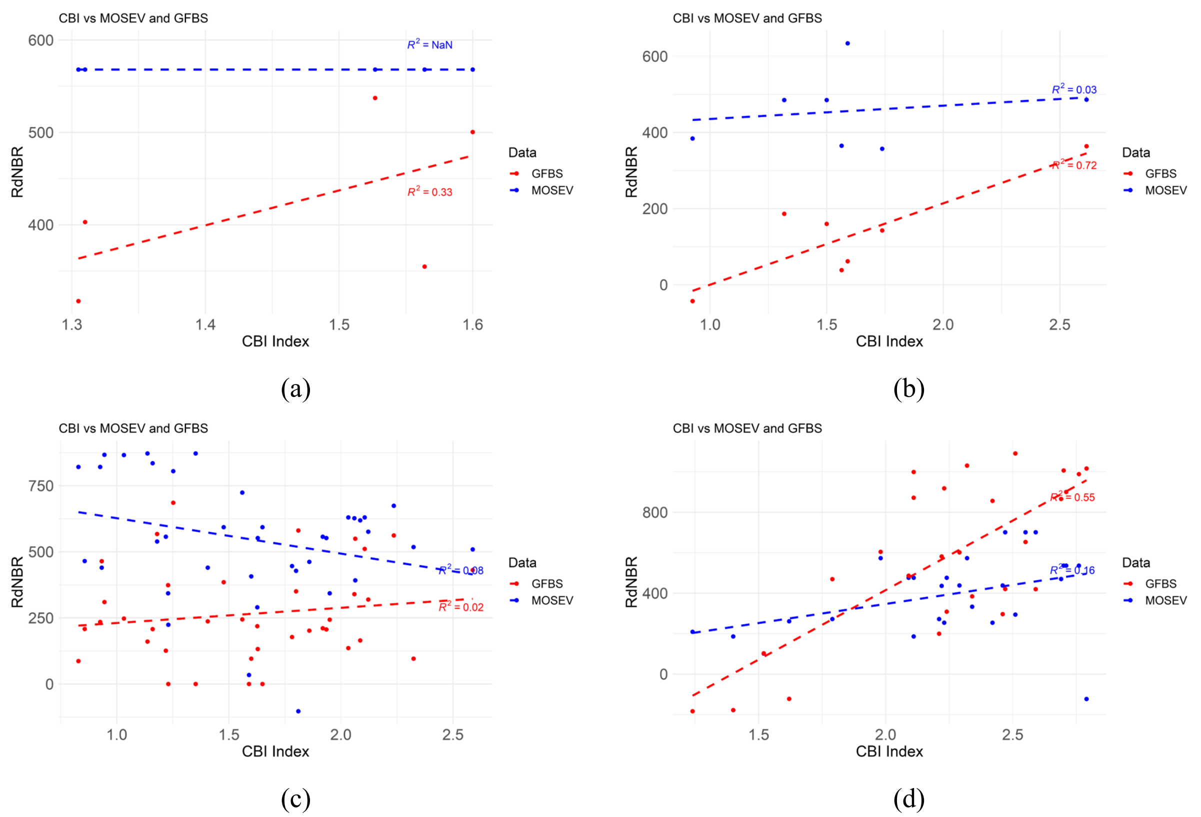

Figure 7. Scatterplots of CBI against RdNBR of GFBS and MOSEV for annual maximum fires in (a) 2004, (b) 2006, (c) 2007, and (d) 2013.

Figure 8 (a) and (b) shows the scatterplots of CBI against GFBS dNBR and MOSEV dNBR, respectively, for all forest fires from 2003 to 2016 over CONUS. Considering all forest fires, we found GFBS dNBR more strongly correlated with CBI (R^2 = 0.4) than MOSEV dNBR (R^2 = 0.08). As for RdNBR, Figure 8 (c) and (d) show the

https://doi.org/10.5194/essd-2023-446
Preprint. Discussion started: 20 December 2023

scatterplots of CBI against GFBS RdNBR and MOSEV RdNBR, respectively, GFBS still performed better than MOSEV when regressed with CBI with an R^2 of 0.31, which was larger than that of MOSEV RdNBR (0.04).

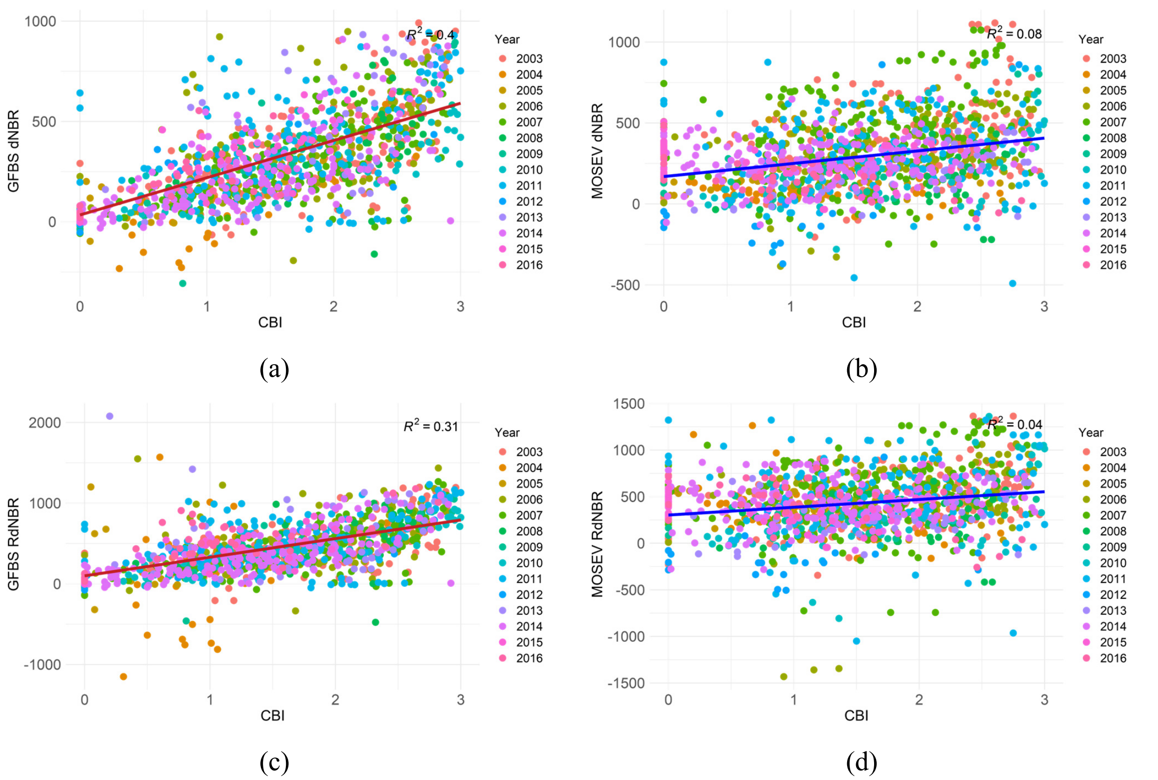

Figure 8. Scatterplots of CBI against (a) dNBR of GFBS, (b) dNBR of MOSEV, (c) RdNBR of GFBS, and (d) RdNBR of MOSEV for all forest fires from 2003 to 2016 over CONUS.

3.3. Comparison of GFBS and MOSEV globally

Figure 9 (a) displays the global spatial distributions of the areas of overlap between the density plots of GFBS dNBR and MOSEV dNBR, which is defined as the area intersected by two probability density functions presented in Figure 4 and Figure 6. The overlapping areas in density plots typically represent the percentage of common values between the distributions of two datasets, which ranges from 0 to 1 with the larger value indicating the two distributions are more likely come from the same distribution. As the figure shows, we found the overlap over most of the world to be above 0.4, indicating a close similarity of 40% between the burn severity information provided, respectively, by GFBS

https://doi.org/10.5194/essd-2023-446
Preprint. Discussion started: 20 December 2023

and MOSEV in these regions. For some regions, like South America, Western Europe, and southeast Australia, the overlap was above 0.6.

In Figure 9 (b), which shows the global distribution of the mean dNBR for each burn pixel derived from GFBS, it is obvious that we found the global spatial heterogeneity of burn severity to be small, with dNBR values around 100 and 200. The exception was Western Europe, where dNBR was above 300. The global distribution of the mean dNBR for each burn pixel derived from MOSEV, as shown in Figure 9 (c), however, indicated a large spatial variability in burn severity. The MOSEV dataset, for example, indicated that the forest fires in north CONUS and Canada should have the average dNBR value above 300, while in the GFBS dataset the average dNBR value was around 100 to 200. The MOSEV dataset also indicated the average dNBR values for forest fires in South Africa and China should be close to or below 0, while in the GFBS dataset they were around 100 to 200.

Figure 9 (d) presents a more detailed comparison between the GFBS dNBR and MOSEV dNBR globally, showing the difference in the mean dNBR for each burn pixel, as calculated by MOSEV dNBR minus GFBS dNBR. Globally, MOSEV data indicated higher forest burn severity over CONUS and Canada as well as southeast Australia than shown by GFBS data. MOSEV data presented lower forest burn severity over Mexico, South Africa, Europe, China, and Southeast Asia. These findings revealed that the forest burn severity information provided by GFBS might be less under- or overestimated than that provided by MOSEV for some fire-prone areas, such as CONUS, as validated in this study. The finding could also be applicable to other regions, including Canada, South Africa, and Australia. This improved accuracy over MOSEV data would support advances in decision making in fire management strategies and ecosystem conservation efforts.

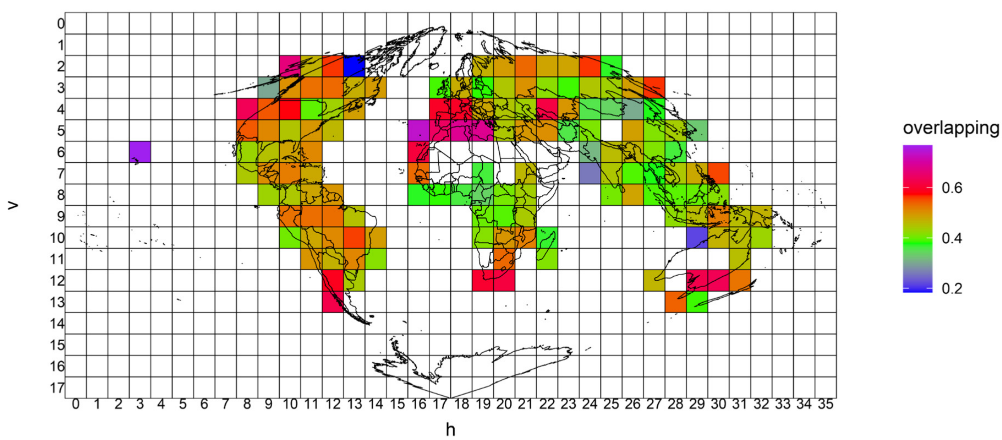

(a)

https://doi.org/10.5194/essd-2023-446
Preprint. Discussion started: 20 December 2023

Open Access Earth System Science Data Discussions

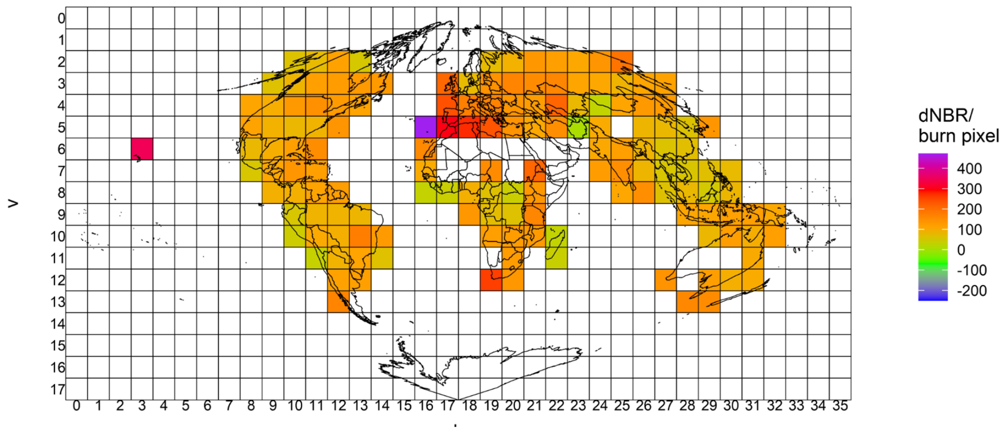

(b)

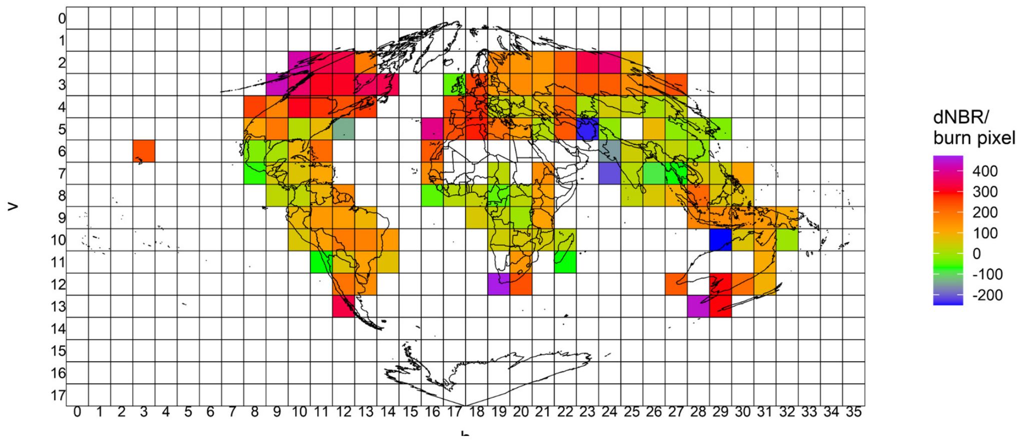

(c)

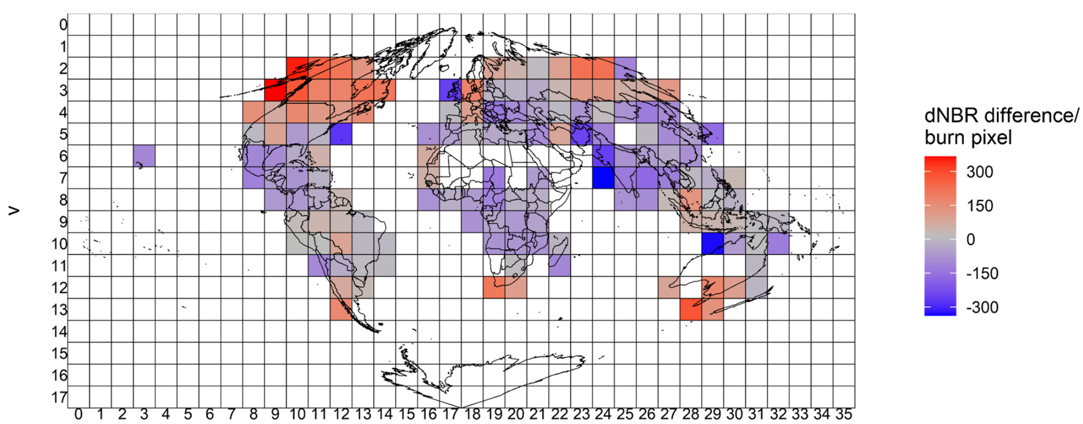

(d)

https://doi.org/10.5194/essd-2023-446
Preprint. Discussion started: 20 December 2023

Figure 9. Global spatial distributions of (a) overlapping areas between the density plots of GFBS dNBR and MOSEV dNBR, (b) the mean dNBR per burn pixel from GFBS, (c) the mean dNBR per burn pixel from MOSEV, and (d) the differences in the mean dNBR per burn pixel between MOSEV and GFBS (MOSEV – GFBS).

4. Discussion

Our GFBS dataset is the first to provide fine spatial resolution (30m) burn severity information for global forest fires from 2003 to 2016. As suggested by the validation against the CBI ground reference, GFBS can capture more spatial variability and provide higher performance than the MOSEV dataset. In addition, GFBS is shown to have less over- or underestimation than MOSEV for some fire-prone areas, like CONUS, Canada, South Africa, and Australia, which could support advances in decision making in fire management strategies and ecosystem conservation efforts.

The difference in the performance of GFBS and MOSEV with respect to burn severity can be attributed to two sources. The first is the spatial resolution. We based GFBS on Landsat (5, 7, and 8) images with a resolution of 30 meters, while MOSEV is based on MODIS Terra MOD09A1 and Aqua MYD09A1 images with a resolution of 500 meters. GFBS dNBR varies from 210 to 310, showing a better correlation with CBI than MOSEV. The coarse resolution of MOSEV could also make it more difficult to capture extreme values, as we found to be the case for the annual maximum forest fires in 2006 over CONUS. GFBS dNBR clearly showed two peaks in the density plot of dNBR at around 100 and 700, representing the low and high severity, respectively. MOSEV dNBR, however, showed only a single peak at around 500, indicating that the extreme low/high values in the 30m grid were averaged in the 500m grid.

The difference in the performances of the two data sets was related to spectrum reflectance information. The NBR is commonly calculated using near-infrared (NIR) and shortwave infrared (SWIR) bands. In MOSEV, the bands used to calculate NBR are NIR: Band 2 (Range: 0.841–0.876 µm) and SWIR: Band 7 (Range: 2.105–2.155 µm). In GFBS, they are Landsat 5 Band 4 (Range: 0.76–0.90 µm) and SWIR: Band 7 (Range: 2.08–2.35 µm); Landsat 7 Band 4 (Range: 0.77–0.90 µm) and SWIR: Band 7 (Range: 2.09-2.35 µm); and Landsat 8 Band 5 (Range: 0.85–0.88 µm) and SWIR: Band 7 (Range: 2.11–2.29 µm). While MODIS and Landsat 8 are close in NIR and SWIR band information, Landsat 5 and 7 both have wider spectrums in NIR and SWIR than MODIS.

One limitation of the GFBS database is related to the relatively long revisit period of Landsat satellites (16 days). This low temporal resolution may impede us from obtaining the dense cloud-free NBR time series that can be indispensable to calculating burn severity indices in regions of persistent cloud cover. This study has shown, however, that using and combining all available Landsat images, including those from Landsat 5, 7, and 8, could significantly improve the probability of obtaining dense cloud-free NBR time series. With the launch of Landsat 9 in September 2021 and other satellites like Sentinel-2 (in June 2015, with a five-day revisit period), it is highly possible that we could build a denser cloud-free NBR time series to calculate burn severity.

https://doi.org/10.5194/essd-2023-446
Preprint. Discussion started: 20 December 2023

A second limitation of GFBS is that it uses different band information varies in spectrum range from Landsat 5, 7, and 8, which might cause data quality to differ across years, while MOSEV uses the same bands in all years, showing better data consistency.

5. Conclusion

We have introduced a newly developed GFBS database, which provides forest burn severity information with global coverage for the period 2003–2016. We identified global forest fires by overlaying the Global Fire Atlas data with the annual land cover data, MCD12Q1, and proposed an automated algorithm for calculating the severity of these fires. The algorithm used the band information from Landsat 5, 7, and 8 surface reflectance imagery to compute the most used burn severity spectral indices (dNBR and RdNBR) with a 30m spatial resolution and provide the output as the GFBS dataset. The validation results over CONUS showed dNBR of GFBS more strongly correlated with CBI (R^2 = 0.4) than dNBR of MOSEV (R^2 = 0.08). RdNBR of GFSS also showed better agreement with CBI (R^2 = 0.31) than RdNBR of MOSEV (R^2 = 0.04). Thus, this database could be more reliable than prior sources of information for future studies of forest burn severity at the global scale in a computationally cost-effective way, as well as for studies to which forest burn severity could be relevant, such as in forest management and CO^2 emissions research.

One future direction for this study will be to extend the GFBS dataset to the present based on updated Global Fire Atlas data or other datasets providing similar burn area and burn date information. A second is to show the similar spatial patterns in presenting burn severity from GFBS and MOSEV dataset, the less over/underestimated GFBS data could serve as an optional input for adjusting the bias in MOSEV data and take the advantage of high spatial resolution of GFBS data, the spatial downscaling of MOSEV data is applicable in regions where GFBS and MOSEV show high consistency.

Competing interests: The authors declare they have no conflict of interest.

Data availability: The GFBS data are freely accessible at https://doi.org/10.5281/zenodo.10037629 (He et al., 2023)

Author contributions: KH and EA designed and organized the manuscript. KH and XS prepared the related materials and ran the models for generating GFBS and the related assessments. XS and EA made contributions to the scientific framework of this study and discussed the interpretation of the results. All authors discussed the results and commented on the manuscript.

Acknowledgments: This research was supported by a National Science Foundation HDR award entitled "Collaborative Research: Near Term Forecast of Global Plant Distribution Community Structure and Ecosystem Function." Kang He received the support of the China Scholarship Council for four years' Ph.D. study at the University of Connecticut (under grant agreement no. 201906320068).

Reference:

Doerr, S.H. and Santín, C., 2016. Global trends in wildfire and its impacts: perceptions versus realities in a changing world. Philosophical Transactions of the Royal Society B: Biological Sciences, 371(1696), p.20150345.

https://doi.org/10.5194/essd-2023-446
Preprint. Discussion started: 20 December 2023

Shukla, P.R., Skea, J., Calvo Buendia, E., Masson-Delmotte, V., Pörtner, H.O., Roberts, D.C., Zhai, P., Slade, R., Connors, S., Van Diemen, R. and Ferrat, M., 2019. IPCC, 2019: Climate Change and Land: an IPCC special report on climate change, desertification, land degradation, sustainable land management, food security, and greenhouse gas fluxes in terrestrial ecosystems.

Dupuy, J.L., Fargeon, H., Martin-StPaul, N., Pimont, F., Ruffault, J., Guijarro, M., Hernando, C., Madrigal, J. and Fernandes, P., 2020. Climate change impact on future wildfire danger and activity in southern Europe: a review. Annals of Forest Science, 77(2), pp.1-24.

Moreira, F., Ascoli, D., Safford, H., Adams, M.A., Moreno, J.M., Pereira, J.M., Catry, F.X., Armesto, J., Bond, W., González, M.E. and Curt, T., 2020. Wildfire management in Mediterranean-type regions: paradigm change needed. Environmental Research Letters, 15(1), p.011001.

Scholes, R.J. and Archer, S.R., 1997. Tree-grass interactions in savannas. Annual review of Ecology and Systematics, 28(1), pp.517-544.

Abreu, R.C., Hoffmann, W.A., Vasconcelos, H.L., Pilon, N.A., Rossatto, D.R. and Durigan, G., 2017. The biodiversity cost of carbon sequestration in tropical savanna. Science advances, 3(8), p.e1701284.

Flannigan, M.D., Stocks, B.J. and Wotton, B.M., 2000. Climate change and forest fires. Science of the total environment, 262(3), pp.221-229.

Nasi, R., Dennis, R., Meijaard, E., Applegate, G. and Moore, P., 2002. Forest fire and biological diversity. UNASYLVA-FAO-, pp.36-40.

Flannigan, M.D., Amiro, B.D., Logan, K.A., Stocks, B.J. and Wotton, B.M., 2006. Forest fires and climate change in the 21 st century. Mitigation and adaptation strategies for global change, 11, pp.847-859.

Jolly, W.M., Cochrane, M.A., Freeborn, P.H., Holden, Z.A., Brown, T.J., Williamson, G.J. and Bowman, D.M., 2015. Climate-induced variations in global wildfire danger from 1979 to 2013. Nature communications, 6(1), p.7537.

Kasischke, E.S. and Turetsky, M.R., 2006. Recent changes in the fire regime across the North American boreal region—Spatial and temporal patterns of burning across Canada and Alaska. Geophysical research letters, 33(9).

Aragão, L.E., Anderson, L.O., Fonseca, M.G., Rosan, T.M., Vedovato, L.B., Wagner, F.H., Silva, C.V., Silva Junior, C.H., Arai, E., Aguiar, A.P. and Barlow, J., 2018. 21st Century drought-related fires counteract the decline of Amazon deforestation carbon emissions. Nature communications, 9(1), p.536.

Archibald, S. and Roy, D.P., 2009, July. Identifying individual fires from satellite-derived burned area data. In 2009 IEEE International Geoscience and Remote Sensing Symposium (Vol. 3, pp. III-160). IEEE.

Hantson, S., Pueyo, S. and Chuvieco, E., 2015. Global fire size distribution is driven by human impact and climate. Global Ecology and Biogeography, 24(1), pp.77-86.

https://doi.org/10.5194/essd-2023-446
Preprint. Discussion started: 20 December 2023

Oom, D., Silva, P.C., Bistinas, I. and Pereira, J.M., 2016. Highlighting biome-specific sensitivity of fire size distributions to time-gap parameter using a new algorithm for fire event individuation. Remote Sensing, 8(8), p.663.

Nogueira, J.M., Ruffault, J., Chuvieco, E. and Mouillot, F., 2016. Can we go beyond burned area in the assessment of global remote sensing products with fire patch metrics?. Remote Sensing, 9(1), p.7.

Laurent, P., Mouillot, F., Yue, C., Ciais, P., Moreno, M.V. and Nogueira, J.M., 2018. FRY, a global database of fire patch functional traits derived from space-borne burned area products. Scientific Data, 5(1), pp.1-12.

Benali, A., Russo, A., Sá, A.C., Pinto, R.M., Price, O., Koutsias, N. and Pereira, J.M., 2016. Determining fire dates and locating ignition points with satellite data. Remote Sensing, 8(4), p.326.

Fusco, E.J., Abatzoglou, J.T., Balch, J.K., Finn, J.T. and Bradley, B.A., 2016. Quantifying the human influence on fire ignition across the western USA. Ecological applications, 26(8), pp.2390-2401.

Chuvieco, E., Yue, C., Heil, A., Mouillot, F., Alonso-Canas, I., Padilla, M., Pereira, J.M., Oom, D. and Tansey, K., 2016. A new global burned area product for climate assessment of fire impacts. Global Ecology and Biogeography, 25(5), pp.619-629.

Rodrigues, M. and Febrer, M., 2018, April. Spatial-temporal modeling of forest fire behavior: modeling fire ignition and propagation from MCD64A1. In EGU General Assembly Conference Abstracts (p. 14568).

Andela, N., Morton, D.C., Giglio, L., Paugam, R., Chen, Y., Hantson, S., Van Der Werf, G.R. and Randerson, J.T., 2019. The Global Fire Atlas of individual fire size, duration, speed and direction. Earth System Science Data, 11(2), pp.529-552.

Keeley, J.E., 2009. Fire intensity, burn severity and burn severity: a brief review and suggested usage. International journal of wildland fire, 18(1), pp.116-126.

Chuvieco, E., Aguado, I., Yebra, M., Nieto, H., Salas, J., Martín, M.P., Vilar, L., Martínez, J., Martín, S., Ibarra, P. and De la Riva, J., 2010. Development of a framework for fire risk assessment using remote sensing and geographic information system technologies. Ecological modelling, 221(1), pp.46-58.

Eidenshink, J., Schwind, B., Brewer, K., Zhu, Z.L., Quayle, B. and Howard, S., 2007. A project for monitoring trends in burn severity. Fire ecology, 3(1), pp.3-21.

Guindon, L., Gauthier, S., Manka, F., Parisien, M.A., Whitman, E., Bernier, P., Beaudoin, A., Villemaire, P. and Skakun, R., 2021. Trends in wildfire burn severity across Canada, 1985 to 2015. Canadian Journal of Forest Research, 51(9), pp.1230-1244.

Alonso-González, E. and Fernández-García, V., 2021. MOSEV: a global burn severity database from MODIS (2000–2020). Earth Syst. Sci. Data 13, 1925–1938.

https://doi.org/10.5194/essd-2023-446
Preprint. Discussion started: 20 December 2023

Key, C.H. and Benson, N.C., 2006. Landscape assessment (LA). FIREMON: Fire effects monitoring and inventory system, 164, pp.LA-1.

Miller, J.D. and Thode, A.E., 2007. Quantifying burn severity in a heterogeneous landscape with a relative version of the delta Normalized Burn Ratio (dNBR). Remote sensing of Environment, 109(1), pp.66-80.

He, K., Shen, X., & Anagnostou, E. N. (2023). A Global Forest Burn Severity Dataset from Landsat Imagery (2003–2016) [Data set]. Zenodo. https://doi.org/10.5281/zenodo.10037629